

All-dielectric meta-holograms with holographic images transforming longitudinally

Qiu Wang, Quan Xu, Xueqian Zhang, Chunxiu Tian, Yuehong Xu, Jianqiang Gu, Zhen Tian, Chunmei Ouyang, Xixiang Zhang, Jianguang Han, and Weili Zhang

ACS Photonics, **Just Accepted Manuscript** • DOI: 10.1021/acsp Photonics.7b01173 • Publication Date (Web): 22 Nov 2017

Downloaded from <http://pubs.acs.org> on December 3, 2017

Just Accepted

“Just Accepted” manuscripts have been peer-reviewed and accepted for publication. They are posted online prior to technical editing, formatting for publication and author proofing. The American Chemical Society provides “Just Accepted” as a free service to the research community to expedite the dissemination of scientific material as soon as possible after acceptance. “Just Accepted” manuscripts appear in full in PDF format accompanied by an HTML abstract. “Just Accepted” manuscripts have been fully peer reviewed, but should not be considered the official version of record. They are accessible to all readers and citable by the Digital Object Identifier (DOI®). “Just Accepted” is an optional service offered to authors. Therefore, the “Just Accepted” Web site may not include all articles that will be published in the journal. After a manuscript is technically edited and formatted, it will be removed from the “Just Accepted” Web site and published as an ASAP article. Note that technical editing may introduce minor changes to the manuscript text and/or graphics which could affect content, and all legal disclaimers and ethical guidelines that apply to the journal pertain. ACS cannot be held responsible for errors or consequences arising from the use of information contained in these “Just Accepted” manuscripts.

All-dielectric meta-holograms with holographic images transforming longitudinally

Qiu Wang[†], Quan Xu[†], Xueqian Zhang[†], Chunxiu Tian[‡], Yuehong Xu[†], Jianqiang Gu[†], Zhen Tian[†], Chunmei Ouyang[†], Xixiang Zhang^{*‡}, Jiaguang Han^{*†}, and Weili Zhang^{*†,§}

[†]Center for Terahertz waves and College of Precision Instrument and Optoelectronics Engineering, Tianjin University and the Key Laboratory of Optoelectronics Information and Technology (Ministry of Education), Tianjin 300072, China.

[‡]Physical Science and Engineering Division, King Abdullah University of Science and Technology, Thuwal 23955-6900, Saudi Arabia.

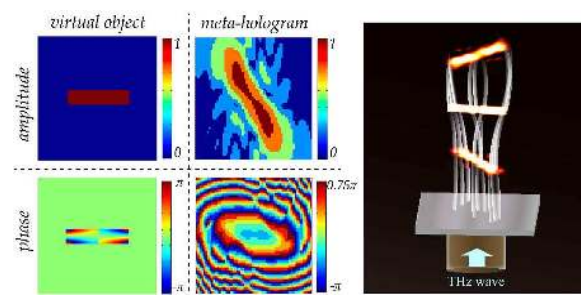
[§]School of Electrical and Computer Engineering, Oklahoma State University, Stillwater, Oklahoma 74078, USA.

ABSTRACT

Metasurfaces are unique subwavelength geometries capable of engineering electromagnetic waves at will, delivering new opportunities for holography. Most previous meta-holograms, so-called phase-only meta-holograms, modulate only the amplitude distribution of a virtual object, and require optimizing techniques to improve the image quality. However, the phase distribution of the reconstructed image is usually overlooked in previous studies, leading to inevitable information loss. Here, we demonstrate all-dielectric meta-holograms that allow tailoring of both the phase and amplitude distributions of virtual objects. Several longitudinal manipulations of the holographic images are theoretically and experimentally demonstrated, including shifting, stretching, and rotating, enabling a large depth of focus. Furthermore, a new meta-hologram with a three-dimensional holographic design method is demonstrated with an even enhanced depth of focus. The proposed meta-holograms offer more freedom in holographic design and open new avenues for designing complex three-dimensional holography.

1
2
3
4 **KEY WORDS:** meta-hologram, all-dielectric metasurface, phase-amplitude modulation,
5
6 three-dimensional, terahertz
7
8
9

10
11 **TOC GRAPHIC**



1
2
3 Holograms record the complete amplitude and phase information of light scattering by an
4
5 object, thus capturing a three-dimensional (3D) image to project. Holography is originally
6
7 proposed by Gabor in 1948.¹ As computer technology and optoelectronics rapidly advance,
8
9 computer-generated holography (CGH) emerges, where holograms are created by numerical
10
11 calculation and reconstructed optically.² CGH has been widely accepted, as it does not
12
13 require real objects and can be applied across the whole electromagnetic spectrum.
14
15 Conventional CGH often uses spatial light modulators (SLMs) as holograms. Recently, the
16
17 adoption of metasurfaces as holograms in CGH has produced high-resolution
18
19 meta-holograms and high efficiency meta-holography.³⁻¹⁵
20
21
22
23
24

25
26 Metasurfaces, which typically consist of a monolayer of subwavelength plasmonic or
27
28 dielectric structures, are simple to fabricate, exhibit relatively low absorption loss, and have
29
30 fascinating electromagnetic characteristics.^{16,17} Metasurfaces can be designed to control the
31
32 polarization, phase, and amplitude of outgoing electromagnetic waves as desired, providing
33
34 an exciting platform for ultrathin optics. Ultrathin metasurfaces have much smaller unit cell
35
36 sizes and thicknesses than their conventional counterparts. Thanks to these unique properties,
37
38 metasurfaces have achieved various intriguing phenomena and applications, such as ultrathin
39
40 flat lenses,¹⁸⁻²² anomalous reflection and refraction,²³⁻²⁶ optical vortex generation,²⁷⁻²⁹ wave
41
42 plates,^{30,31} and meta-holography.³⁻¹⁵ Plasmonic metasurfaces easily support electromagnetic
43
44 resonances; however, they typically suffer from low efficiency due to ohmic loss. Composed
45
46 of high refractive index resonators, dielectric metamaterial unit cells use Mie resonances to
47
48 generate electric and magnetic resonances with dramatically improved efficiency.^{32,33}
49
50
51
52
53

54
55 Most past demonstrations of meta-holography have used phase-only holograms, where
56
57
58
59
60

1
2
3
4 optimizing techniques such as the Gerchberg-Saxton method were adopted to improve the
5
6 holographic image quality.³⁴⁻³⁶ However, these optimization techniques cause the phase
7
8 distribution of the reconstructed image to become irregular and uncontrollable. As amplitude
9
10 and phase are two fundamental characteristics of electromagnetic waves, the uncontrollable
11
12 phase distribution clearly constrains the holographic design. Rather than employing
13
14 optimizing techniques, a new approach could provide simultaneous control of amplitude and
15
16 phase of each pixel in the metasurface^{7,37} to achieve high quality holographic images. With
17
18 this approach, both amplitude and phase information of virtual objects can be reconstructed.
19
20 However, this meta-hologram by adopting single-layer plasmonic resonators⁷ has been
21
22 difficult to move beyond the limitations in the inherent Ohmic losses and the orthogonal
23
24 polarization conversion efficiency. A higher efficiency is required in practical applications of
25
26 the simultaneous amplitude and phase control technique. Also, only amplitude distribution of
27
28 the virtual object is considered in that work, while the phase distribution is kept constant.
29
30 This is just like many other studies on meta-holography, where the main concern is the
31
32 quality of the reconstructed intensity distribution, since the phase information cannot be
33
34 recorded directly by the eyes or detectors. The effect of engineering both the phase and
35
36 amplitude distributions of virtual objects in meta-holography has not been further studied yet.
37
38
39
40
41
42
43
44

45 In this article, we propose and demonstrate all-dielectric meta-holograms that
46
47 continuously transform holographic images along the longitudinal direction by engineering
48
49 both the phase and amplitude distributions of the virtual objects in the terahertz regime.
50
51 Dielectric cubic silicon resonators are used as basic unit cells to achieve a simultaneous
52
53 multi-level modulation of the amplitude and phase distributions on the holograms with
54
55
56
57
58
59
60

1
2
3 relatively high efficiency. Fiber-based near-field scanning terahertz microscopy (FNSTM) is
4 employed in the experimental measurements with a high scanning speed and high resolution.
5
6 The shifting, stretching, and rotating of the images along the direction of electromagnetic
7 wave propagation are theoretically and experimentally demonstrated, and indicate a large
8 depth of focus (DOF). The DOF, that illustrates the tolerance of a hologram in the position
9 where an image is detected, is a very important parameter and reflects the longitudinal
10 resolution. The DOF of our hologram is proven to be larger than that of the phase-only
11 hologram with optimization. Moreover, a new design approach for three dimensional (3D)
12 holograms is proposed with further enhanced DOF. The proposed meta-holograms allow
13 more freedom in the holographic design process through engineering both of the phase and
14 amplitude distributions of the virtual 3D objects. The larger DOF accelerates the pace of
15 meta-holography towards practical applications.
16
17
18
19
20
21
22
23
24
25
26
27
28
29
30
31

32 33 34 35 **DESIGN**

36
37 Here, subwavelength silicon pillar resonators are employed as basic unit cells, as shown
38 in Figure 1a. The pillars are made from 150 μm thick high-resistivity silicon and patterned on
39 a 2 mm thick high-resistivity silicon substrate. According to the effective media theory, a
40 large effective refractive index leads to a slow electromagnetic wave speed, whose direction
41 of propagation can be defined as the slow axis and the fast axis is thus along the orthogonal
42 direction, as illustrated in Figure 1b. When the optical path difference between the two
43 polarized components along the slow axis and the fast axis is equal to half of a wavelength,
44
45
46
47
48
49
50
51
52
53
54
55
56
57
58
59
60

1
2
3 the linearly polarized incidence converts nearly completely into the orthogonal polarized
4
5 component, where the silicon pillar serves as a half-waveplate.
6
7

8 The performance of the all-dielectric meta-holography is numerically simulated using a
9
10 commercial software, CST Microwave Studio. Four silicon pillars with approximately 0.9
11
12 amplitude transmission and a $\pi/4$ phase-shift interval of the outgoing y -polarized electric field
13
14 components E_y are selected under 1.0 THz and an x -polarized incident plane wave. Their
15
16 geometric parameters are $(a, b) = (48 \mu\text{m}, 115 \mu\text{m}), (40 \mu\text{m}, 112 \mu\text{m}), (35 \mu\text{m}, 93 \mu\text{m}),$ and
17
18 $(24 \mu\text{m}, 101.5 \mu\text{m}),$ respectively. By incorporating the additional x -axis-mirrored unit cells,
19
20 eight silicon pillar resonators are obtained, composing a phase shift ranging from zero to 2π
21
22 and nearly the same transmissions, as shown in Figure 1c. All eight silicon pillars are
23
24 designed with same $(P, h) = (130 \mu\text{m}, 150 \mu\text{m})$ for ease of fabrication. Based on the
25
26 coordinate system transformation theory, when a silicon pillar rotates around the z -axis, the
27
28 phase shift of the outgoing y -polarized component remains constant under an x -polarized
29
30 incidence, except for a π jump when the slow axis or the fast axis passes the x -axis.
31
32 Meanwhile, the amplitude of the y -polarized electric field component $|E_y|$ is proportional to
33
34 $|\sin(2\theta)|$, where θ represents the orientation of the slow axis relative to the x -axis. As θ varies
35
36 from -90° to 90° in a 5° interval, the numerically simulated results of the amplitude and phase
37
38 shifts of the outgoing y -polarized component E_y for the first silicon pillar of the eight unit
39
40 cells remain consistent with our expectations. Thus, the simultaneous modulation of phase
41
42 and amplitude in each pixel of the metasurface has been achieved with high efficiency.
43
44
45
46
47
48
49
50
51
52
53
54
55
56
57
58
59
60

RESULTS

Most of the meta-holograms demonstrated before only focus on the amplitude distributions of holographic images. Many optimizing techniques, including the Gerchberg-Saxton method, are employed in these phase-only holograms to improve the image quality; however, the trade-off is that the phase distribution becomes uncontrollable. Here, by elaborately engineering both the phase and amplitude distributions of two-dimensional (2D) virtual objects, several manipulations of the holographic images along the longitudinal direction (z -axis), namely different image transformations in 3D space are achieved as presented in detail below.

Longitudinal manipulations of the holographic images: shifting

An image of the letter “T” with a constant amplitude is designed to appear in the plane $z = 6$ mm. The size of the observed region is 8×8 mm², as shown in Figure 2a. The horizontal and vertical rectangles of the “T” are designed to move in opposite directions along the x -axis. Thus, the normalized electric field distribution of the virtual object is

$$E(x, y) = \begin{cases} \exp(ik_1x), & x \in [-2, 2], y \in [1.5, 2.5] \\ \exp(-ik_1x), & x \in [-0.5, 0.5], y \in [-2.5, 1.5] \\ 0, & \text{else} \end{cases} \quad (mm) \quad (1)$$

Here, we let $k_1 = 2\pi$ rad/mm. The electric field phase distribution of the virtual object is shown in Figure 2b.

To design the corresponding meta-hologram, the Rayleigh-Sommerfeld diffraction theory is applied. After normalization, the linear partition method is employed to discretize the amplitude into five levels (0, 0.25, 0.5, 0.75, or 1). By utilizing silicon pillar resonators as

1
2
3 the basic unit pixels, the simultaneous eight-level phase and five-level amplitude modulation
4 is achieved. The electric field amplitude and phase distributions of the meta-hologram can be
5
6 seen in Figure 2c and d, respectively. Composed by 61×61 pixels, the dielectric
7
8 meta-hologram is fabricated by conventional deep reactive ion etching (DRIE), whose partial
9
10 scanning electron microscopy image is shown in Figure 2e. Thus, the size of the
11
12 meta-hologram is also approximately $8 \times 8 \text{ mm}^2$.
13
14
15
16
17

18 The Rayleigh-Sommerfeld diffraction theory is applied again in the image
19
20 reconstruction. The numerically simulated electric field amplitude distributions $|E_y|$ under 1.0
21
22 THz at different locations ranging from $z = 4$ to 8 mm are shown in Figure 2f. The “T” image
23
24 appears at $z = 6$ mm, and then changes into “┌” and “└” at $z = 4$ mm and $z = 8$ mm,
25
26 respectively.
27
28
29

30 FNSTM is employed in the experimental demonstrations. The measured y -polarized
31
32 electric field amplitude distributions $|E_y|$ under 1.0 THz and x -polarized illumination at
33
34 different locations along the z -axis are shown in Figure 2g. The electric field is detected at
35
36 0.25 mm intervals from -4 to 4 mm in both the x and y directions, and at a 1 mm interval from
37
38 4 to 8 mm in the z direction. The shifting of the two “T” components along the z -axis can be
39
40 clearly seen with good image quality from $z = 4$ to 8 mm, which coincides well with the
41
42 simulated results in terms of image size, profile, location, and relative amplitude distribution,
43
44 demonstrating good control over shifting in the meta-hologram. There’s a little quality
45
46 difference between the reconstructed vertical rectangle and the reconstructed horizontal
47
48 rectangle, especially in the edges of these rectangles, which is mainly due to the information
49
50 loss caused by the limited hologram size. As can be seen in Figure 2c, the right edge of the
51
52
53
54
55
56
57
58
59
60

1
2
3 horizontal rectangular region in the hologram is “cut off” by the boundary of the hologram,
4
5 while the edges of the vertical one are overall exhibited in the hologram. The missing
6
7 information will mainly affect its corresponding image region, considering that the image
8
9 plane is just 6 mm away from the hologram (twentyfold wavelength for 1 THz). That’s why
10
11 the main difference appears in the edges of the rectangles and why the left edge of the
12
13 horizontal rectangle exhibits better than the right edge. The quality of the reconstructed
14
15 horizontal rectangle will be better if the hologram is large enough to contain all the
16
17 amplitude-not-zero pixels. Besides, the speed of the image shifting can be easily manipulated
18
19 by varying k_1 . The measured transmission efficiency, defined as the ratio between the
20
21 measured y -polarized terahertz power in the “T” region at $z = 6$ mm and the input power,
22
23 reaches 16.3 % when employing the dielectric silicon pillar resonators. The corresponding
24
25 simulated transmission efficiency of the silicon pillars is 18.8 %, which is much higher than
26
27 that of the single-layer transmission-type plasmonic structures with simultaneous phase and
28
29 amplitude modulation (6.4 % in our previous work).⁷ The good holographic image quality
30
31 and the high efficiency promise practical applications in meta-holography.
32
33
34
35
36
37
38
39
40
41
42

43 **Longitudinal manipulations of the holographic images: stretching**

44
45 The methods for meta-hologram design, sample fabrication, numerical simulation, and
46
47 experimental measurements are the same as in the shifting exercise. The same “T” with a
48
49 constant amplitude is designed to appear in the plane $z = 6$ mm, as shown in Figure 3a. The
50
51 image is designed to stretch along the z -axis, so the normalized electric field distribution of
52
53 the virtual object is
54
55
56
57
58
59
60

$$E(x, y) = \begin{cases} \exp(ik_2|x|), & x \in [-2, 2], y \in [1.5, 2.5] \\ \exp[ik_2(2-y)], & x \in [-0.5, 0.5], y \in [-2.5, 1.5] \\ 0, & \text{else} \end{cases} \quad (mm) \quad . \quad (2)$$

Here, we let $k_2 = \pi$ rad/mm. The electric field phase distribution of the virtual object is shown in Figure 3b.

The electric field amplitude and phase distributions of the meta-hologram are exhibited in Figure 3c and d, where the eight-level phase and five-level amplitude modulations are also employed. The simulated and measured amplitude distributions of the y -polarized electric field component under an x -polarized normal incidence at different locations along the z -axis are shown in Figure 3f and g. The simulated and measured results are in good agreement, exhibiting a stretching effect along the z -axis with a range from $z = 4$ to 8 mm. The holographic image “T” becomes smaller as the distance from the meta-hologram increases, which is the opposite of conventional optical imaging behavior. The simulated magnification between the image profiles at planes $z = 4$ mm and $z = 8$ mm is 1.33 along the x direction and 1.17 along the y direction, and the measured magnification is 1.38 and 1.10, respectively. The magnification can be easily controlled by changing k_2 . The measured and simulated efficiencies for this meta-hologram are 14.5 % and 19.6 %, respectively. Note that for the shifting and stretching manipulations, the virtual objects are designed with the same amplitude distributions (the letter “T”) and different phase distributions. Completely different longitudinal exhibitions of holographic images are achieved, which overall exhibit different 3D distributions, indicating the functionality of incorporating phase control into the virtual object.

Longitudinal manipulations of the holographic images: rotating

The virtual object in this experiment is a rectangle with a constant amplitude in the plane $z = 6$ mm, as shown in Figure 4a. The rectangle is designed to be capable of rotating along the z -axis, and every point should have the same space angular velocity ω_0 for image stability. Under the cylindrical coordinate system, when a point (r, θ, z) moves to its next location $(r+dr, \theta+d\theta, z+dz)$, we know that $v_r/c = k_r/k$. Here v_r and k_r represent the space linear velocity component and the wave vector component in the $r\theta$ -plane, respectively; c and k are the velocity of light and wave vector in vacuum, respectively; $k_r = d\phi/dl$, where $d\phi$ and dl are differential phase shift and distance between the two points, respectively. So we can get $v_r = cd\phi/kdl$. Since $v_r = \omega_0 r$ and $dl = rd\theta$, we can obtain $d\phi = \omega r^2 d\theta$, where $\omega = \omega_0 k/c$ is a constant. After integration, the final phase distribution can be obtained as $\phi = \omega r^2 \theta$. Thus, the normalized electric field distribution of the virtual object is

$$E(x, y) = \begin{cases} \exp[i\omega(x^2 + y^2) \arctan \frac{y}{x}], & x \in [-2, 2], y \in [-0.4, 0.4] \\ 0, & \text{else} \end{cases} \quad (mm) \quad (3)$$

Here, we let $\omega = 4.5 \text{ mm}^{-2}$. The electric field phase distribution of the virtual object is shown in Figure 4b.

Similarly, the electric field amplitude and phase distributions of the meta-hologram, partial scanning electron microscopy image, and the simulated and measured electric field amplitude distributions are shown in Figure 4c-g. Satisfactory rotating is observed, where the simulated rotation angle of the profile of the rectangle from $z = 3$ to 9 mm is 79° , and the measured result is 78° . The rotation angle can be controlled by varying ω . The measured electric field amplitude distributions are in good coincidence with the simulations, including

1
2
3 the image size, profile, orientation angle, and relative amplitude distribution, which
4
5 demonstrates the good rotating manipulation of the holographic images. In addition, the
6
7 measured and simulated efficiencies for this meta-hologram are 8.6 % and 11.6 %,
8
9 respectively.
10
11
12
13
14

15 **Meta-holography with a large DOF**

16
17
18 Our results indicate that a large DOF can be obtained with the proposed holographic
19
20 design approach without the use of optimizing techniques. Irregular phase distribution from
21
22 optimizing techniques leads to poor directivity along the propagation direction, which would
23
24 also reduce the DOF. To further investigate the DOF of different meta-holograms, we design
25
26 three meta-holograms. One is a phase-only meta-hologram optimized by the
27
28 Gerchberg-Saxton method. The second is the meta-hologram of our design with simultaneous
29
30 eight-level phase and five-level amplitude modulation. Each of the two meta-holograms is
31
32 designed to reconstruct a 2D virtual object with a constant amplitude distribution “T” located
33
34 at $z = 6$ mm, which is the same with Figure 2a. A constant phase distribution of the 2D virtual
35
36 object is designed for the second meta-hologram with simultaneous phase and amplitude
37
38 modulation; however, the 2D virtual object’s phase distribution of the phase-only hologram is
39
40 uncontrollable and unable to be designed. Third, we propose 3D holographic design approach
41
42 to achieve an even larger DOF, where the virtual object is a 3D “T” profile from $z = 2$ to 10
43
44 mm with a constant amplitude, as shown in Figure 5a. The phase distribution is a constant in
45
46 each xy -plane, but a $k \times z$ phase shift is designed along the z -axis, as shown in Figure 5b. Here,
47
48 we let k equal the wave vector in an electromagnetic wave vacuum under 1.0 THz. The
49
50
51
52
53
54
55
56
57
58
59
60

1
2
3
4 Rayleigh-Sommerfeld diffraction theory is used and by sum of the contributions of all
5
6 xy -planes from $z = 2$ to 10 mm, the electric field distribution in this 3D designed
7
8 meta-hologram is obtained. Simultaneous eight-level phase and five-level amplitude
9
10 modulation is employed to construct this 3D designed meta-hologram.
11
12

13
14 The measured electric field amplitude distributions of the three meta-holograms under
15
16 1.0 THz are shown in Figure 6a-m. In the results of the phase-only meta-hologram, the “T”
17
18 begins to “split” at $z = 5$ mm and to “granulate” at $z = 7$ mm. In both the meta-hologram with
19
20 simultaneous phase and amplitude modulation and the 3D designed meta-hologram, the
21
22 image quality along the z -axis is extensively enhanced. The 3D designed meta-hologram
23
24 shows even better imaging results than the other two meta-holograms at $z = 2$ mm and $z = 10$
25
26 mm in particular, demonstrating the enhanced DOF of the 3D holographic design approach.
27
28 The different DOF character of these three meta-holograms can be more clearly seen in the
29
30 simulated holographic imaging results shown in Figure S1 (See Supplementary Note 1). The
31
32 measured efficiencies of the phase-only meta-hologram, the meta-hologram with
33
34 simultaneous phase and amplitude modulation, and the 3D designed meta-hologram are
35
36 44.5 %, 13.7 %, and 13.3 %, respectively. Their corresponding simulated efficiencies are
37
38 65.1 %, 17.2 %, and 15.4 %, respectively.
39
40
41
42
43
44

45
46 Given the Strehl ratio in conventional optics, the DOF in holography can be defined as
47
48 the longitudinal range of the image region in which the integral intensity is more than 80 %
49
50 of the integral intensity in the designed focal plane. Experimentally, it is time-consuming and
51
52 extremely difficult to measure the precise DOF as scanning detection is adopted in the
53
54 xy -plane, which is quite different from the charge coupled device (CCD) detection method
55
56
57
58
59
60

1
2
3 used in the visible regime. Therefore, numerical simulations are employed for the quantitative
4 analysis of DOF. The simulated results for the DOF are 2.8 mm (from $z = 5.3$ to 8.1 mm) for
5 the phase-only meta-hologram, 5.0 mm (from $z = 3.8$ to 8.8 mm) for the meta-hologram, and
6 7.9 mm (from $z = 2.7$ to 10.6 mm) for the 3D designed meta-hologram. The simulated and
7 measured results demonstrate that the meta-hologram with simultaneous phase and amplitude
8 modulation has a larger DOF than the phase-only meta-hologram, and that the 3D designed
9 meta-hologram exhibits even further improvement. In addition, the DOF is directly
10 proportional to the object distance and inversely proportional to the aperture. Considering the
11 small object distance (6 mm) and the large size of the meta-hologram ($8 \times 8 \text{ mm}^2$), it is very
12 exciting to realize a 7.9 mm DOF with the 3D design approach. Regarding to the large DOF,
13 we emphasize here that it is very helpful to obtain good images in a long range, which can
14 make the hologram become more robust in real applications. However, for some other 3D
15 holograms, such as irrelevant images at different plane, the large DOF may become crosstalk
16 at other imaging plane in a sense. In that case, one needs other methods to optimize the phase
17 distribution of each virtual image to restrain the crosstalk. By combining the iterative
18 multi-plane holography algorithm with our design method, it might be possible to suppress
19 the crosstalk among different imaging planes if we elaborately design proper initial phase
20 distributions of the multi-plane images to make them capable of propagating approximately
21 from one to the next.

22 23 24 25 26 27 28 29 30 31 32 33 34 35 36 37 38 39 40 41 42 43 44 45 46 47 48 49 50 51 52 **CONCLUSION** 53 54 55 56 57 58 59 60

1
2
3 We demonstrate a new meta-hologram design method by engineering both the phase and
4 amplitude distributions of a virtual object. Relatively high efficiency is obtained by
5 employing dielectric silicon pillar resonators as the basic unit pixels. The shifting, stretching,
6 and rotating of holographic images along the longitudinal direction (z -axis) are demonstrated
7 both theoretically and experimentally, indicating the additional freedom in our holographic
8 design approach and suggesting further manipulation possibilities. The clear holographic
9 images along the propagation direction also indicate a large DOF. A comparison of the DOF
10 of a phase-only meta-hologram, a meta-hologram with simultaneous amplitude and phase
11 control, and a new meta-hologram with 3D holographic design approach confirm that the 3D
12 designed meta-hologram has a much larger DOF than other meta-holograms.

13
14
15 Compared with the phase-only meta-holograms that achieve multi-plane images or 3D
16 images, our both phase and amplitude modulated meta-holograms by engineering both the
17 phase and amplitude distributions of a virtual object can uniquely achieve holographic images
18 continuously transforming along the longitudinal direction in a long range with even no
19 crosstalk. Besides, our design approach is direct and the algorithm is simple and timesaving.
20 Furthermore, from the perspective of information theory, the meta-holograms with both
21 phase and amplitude modulation contain more degree of freedom and thus, contain more
22 information. Hence, they can be designed to realize more complex and flexible holographic
23 images. It is believed that the proposed holographic design approach provides a new method
24 for 3D holographic imaging and has many prospects in practical applications.

25 26 27 28 29 30 31 32 33 34 35 36 37 38 39 40 41 42 43 44 45 46 47 48 49 50 51 52 53 54 55 **METHODS** 56 57 58 59 60

1
2
3 **Sample fabrication.** All the meta-holograms are fabricated by using conventional
4 lithography together with deep reactive ion etching. First, the 2 mm thick double-side
5 polished high-resistivity silicon wafer is sputtered with a 10 nm thick chromium layer and
6 then spin-coated with a 7 μm thick layer of photoresist (AZ2070). Next, by conventional
7 photolithography, the left photoresist and the chromium become a double layer of protection
8 above the silicon pillars. Then, conventional deep reactive ion etching is employed to make
9 the silicon pillars with 150 μm thickness. Finally, the remaining photoresist and the remaining
10 chromium are cleaned off separately.
11
12
13
14
15
16
17
18
19
20
21

22 **Experimental Characterization.** FNSTM is employed in the experimental demonstrations
23 for its high scanning speed and high resolution. Detailed description of FNSTM can be found
24 in our previous work.³⁸ Here, only the y -polarized electric field component is measured with
25 an x -polarized illumination. The electric field is detected at 0.25 mm intervals from -4 to 4
26 mm in both the x and y directions. It is further detected at a 1 mm interval for longitudinal
27 manipulation measurements and a 2 mm interval for DOF characterizations in the z direction.
28
29
30
31
32
33
34
35
36
37
38
39
40
41
42

43 ASSOCIATE CONTENT

44 Supporting Information

- 45 1. Simulated results of the three meta-holograms with different DOF.
46
47
48
49

50 AUTHOR INFORMATION

51 Corresponding Authors

52 *Email: jiaghan@tju.edu.cn.

53 *Email: xixiang.zhang@kaust.edu.sa.

54 *Email: weili.zhang@okstate.edu.
55
56
57
58
59
60

Notes

The authors declare no competing financial interest.

ACKNOWLEDGEMENT

This work was supported by the National Natural Science Foundation of China (Grant Nos. 61422509, 61735012, 61427814, 61420106006, and 61605143), the National Key Basic Research Special Foundation of China (Grant No. 2014CB339800), the Program for Changjiang Scholars and Innovative Research Team in Universities (Grant No. IRT13033), and the U. S. National Science Foundation (Grant No. ECCS-1232081).

REFERENCE

- (1) Gabor, D. A New Microscopic Principle. *Nature* **1948**, *161*, 777-778.
- (2) Lohmann, A. W.; Paris, D. P. Binary Fraunhofer Holograms, Generated by Computer. *Appl. Optics* **1967**, *6*, 1739-1748.
- (3) Mueller, J. P. B.; Rubin, N. A.; Devlin, R. C.; Groever, B.; Capasso, F. Metasurface Polarization Optics: Independent Phase Control of Arbitrary Orthogonal States of Polarization. *Phys. Rev. Lett.* **2017**, *118*, 113901.
- (4) Xie, Z.; Lei, T.; Si, G.; Wang, X.; Lin, J.; Min, C.; Yuan, X. Meta-Holograms with Full Parameter Control of Wavefront over a 1000 nm Bandwidth. *ACS Photonics* **2017**, *4*, 2158-2164.
- (5) Ye, W.; Zeuner, F.; Li, X.; Reineke, B.; He, S.; Qiu, C. W.; Liu, J.; Wang, Y.; Zhang, S.; Zentgraf, T. Spin and Wavelength Multiplexed Nonlinear Metasurface Holography. *Nat. Commun.* **2016**, *7*, 11930.

- 1
2
3
4 (6) Li, X.; Chen, L.; Li, Y.; Zhang, X.; Pu, M.; Zhao, Z.; Ma, X.; Wang, Y.; Hong, M.; Luo,
5
6 X. Multicolor 3D Meta-Holography by Broadband Plasmonic Modulation. *Sci. Adv.*
7
8 **2016**, *2*, e1601102.
9
- 10
11 (7) Wang, Q.; Zhang, X.; Xu, Y.; Gu, J.; Li, Y.; Tian, Z.; Singh, R.; Zhang, S.; Han, J.;
12
13 Zhang, W. Broadband Metasurface Holograms: toward Complete Phase and Amplitude
14
15 Engineering. *Sci. Rep.* **2016**, *6*, 32867.
16
17
- 18 (8) Huang, K.; Dong, Z.; Mei, S.; Zhang, L.; Liu, Y.; Liu, H.; Zhu, H.; Teng, J.;
19
20 Luk'yanchuk, B.; Yang, J. K. W.; Qiu, C. W. Silicon Multi-Meta-Holograms for the
21
22 Broadband Visible Light. *Laser Photonics Rev.* **2016**, *10*, 500-509.
23
24
- 25 (9) Zhang, L.; Mei, S.; Huang, K.; Qiu, C. W. Advances in Full Control of Electromagnetic
26
27 Waves with Metasurfaces. *Adv. Optical Mater.* **2016**, *4*, 818-833.
28
29
- 30 (10) Huang, L.; Mühlenbernd, H.; Li, X.; Song, X.; Bai, B.; Wang, Y.; Zentgraf, T.
31
32 Broadband Hybrid Holographic Multiplexing with Geometric Metasurfaces. *Adv. Mater.*
33
34 **2015**, *27*, 6444-6449.
35
36
- 37 (11) Zheng, G.; Mühlenbernd, H.; Kenney, M.; Li, G.; Zentgraf, T.; Zhang, S. Metasurface
38
39 Holograms Reaching 80% Efficiency. *Nat. Nanotechnol.* **2015**, *10*, 308-312.
40
41
- 42 (12) Huang, Y. W.; Chen, W. T.; Tsai, W. Y.; Wu, P. C.; Wang, C. M.; Sun, G.; Tsai, D. P.
43
44 Aluminum Plasmonic Multicolor Meta-Hologram. *Nano Lett.* **2015**, *15*, 3122-3127.
45
46
- 47 (13) Chen, W. T.; Yang, K. Y.; Wang, C. M.; Huang, Y. W.; Sun, G.; Chiang, I. D.; Liao, C.
48
49 Y.; Hsu, W. L.; Lin, H. T.; Sun, S.; Zhou, L.; Liu, A. Q.; Tsai, D. P. High-Efficiency
50
51 Broadband Meta-Hologram with Polarization-Controlled Dual Images. *Nano Lett.* **2013**,
52
53 *14*, 225-230.
54
55
56
57
58
59
60

- 1
2
3
4 (14) Ni, X.; Kildishev, A. V.; Shalaev, V. M. Metasurface Holograms for Visible Light. *Nat.*
5
6 *Commun.* **2013**, *4*, 2807.
7
- 8 (15) Huang, L.; Chen, X.; Mühlenbernd, H.; Zhang, H.; Chen, S.; Bai, B.; Tan, Q.; Jin, G.;
9
10 Cheah, K. W.; Qiu, C. W.; Li, J.; Zentgraf, T.; Zhang, S. Three-Dimensional Optical
11
12 Holography Using a Plasmonic Metasurface. *Nat. Commun.* **2013**, *4*, 2808.
13
14
- 15 (16) Kildishev, A. V.; Boltasseva, A.; Shalaev, V. M. Planar Photonics with Metasurfaces.
16
17 *Science* **2013**, *339*, 1232009.
18
19
- 20 (17) Meinzer, N.; Barnes, W. L.; Hooper, I. R. Plasmonic Meta-Atoms and Metasurfaces
21
22 *Nat. Photon.* **2014**, *8*, 889-898.
23
24
- 25 (18) Khorasaninejad, M.; Chen, W. T.; Oh, J.; Capasso, F. Super-Dispersive off-Axis
26
27 Meta-Lenses for Compact High Resolution Spectroscopy. *Nano Lett.* **2016**, *16*,
28
29 3732-3737.
30
31
- 32 (19) Arbabi, A.; Ball, A. J.; Bagheri, M.; Faraon, A. Subwavelength-Thick Lenses with High
33
34 Numerical Apertures and Large Efficiency based on High-Contrast Transmitarrays *Nat.*
35
36 *Commun.* **2015**, *6*, 7069.
37
38
39
- 40 (20) Wang, Q.; Zhang, X.; Xu, Y.; Tian, Z.; Gu, J.; Yue, W.; Zhang, S.; Han, J.; Zhang, W. A
41
42 Broadband Metasurface-Based Terahertz Flat-Lens Array. *Adv. Optical Mater.* **2015**, *3*,
43
44 779-785.
45
46
- 47 (21) Wang, Q.; Rogers, E. T. F.; Gholipour, B.; Wang, C. M.; Yuan, G.; Teng, J.; Zheludev,
48
49 N. I. Optically Reconfigurable Metasurfaces and Photonic Devices based on Phase
50
51 Change Materials. *Nat. Photon.* **2016**, *10*, 60-65.
52
53
54
55
56
57
58
59
60

- 1
2
3
4 (22) Chen, B. H.; Wu, P. C.; Su, V. C.; Lai, Y. C.; Chu, C. H.; Lee, I. C.; Chen, J. W.; Chen,
5
6 Y. H.; Lan, Y. C.; Kuan, C. H.; Tsai, D. P. GaN Metalens for Pixel-Level Full-Color
7
8 Routing at Visible Light. *Nano Lett.* **2017**, *17*, 6345-6352.
9
- 10 (23) Ni, X.; Emani, N. K.; Kildishev, A. V.; Boltasseva, A.; Shalaev, V. M. Broadband Light
11
12 Bending with Plasmonic Nanoantennas. *Science* **2012**, *335*, 427-427.
13
14
- 15 (24) Sun, S.; Yang, K. Y.; Wang, C. M.; Juan, T. K.; Chen, W. T.; Liao, C. Y.; He, Q.; Xiao,
16
17 S.; Kung, W. T.; Guo, G. Y.; Zhou, L.; Tsai, D. P. High-Efficiency Broadband
18
19 Anomalous Reflection by Gradient Meta-Surfaces. *Nano Lett.* **2012**, *12*, 6223-6229.
20
21
- 22 (25) Grady, N. K.; Heyes, J. E.; Chowdhury, D. R.; Zeng, Y.; Reiten, M. T.; Azad, A. K.;
23
24 Taylor, A. J.; Dalvit, D. A. R.; Chen, H. T. Terahertz Metamaterials for Linear
25
26 Polarization Conversion and Anomalous Refraction. *Science* **2013**, *340*, 1304-1307.
27
28
- 29 (26) Zhang, X.; Tian, Z.; Yue, W.; Gu, J.; Zhang, S.; Han, J.; Zhang, W. Broadband
30
31 Terahertz Wave Deflection based on C-Shape Complex Metamaterials with Phase
32
33 Discontinuities. *Adv. Mater.* **2013**, *25*, 4567-4572.
34
35
- 36 (27) Yu, N.; Genevet, P.; Kats, M. A.; Aieta, F.; Tetienne, J. P.; Capasso, F.; Gaburro, Z.
37
38 Light Propagation with Phase Discontinuities: Generalized Laws of Reflection and
39
40 Refraction. *Science* **2011**, *334*, 333-337.
41
42
- 43 (28) Yang, Y.; Wang, W.; Moitra, P.; Kravchenko, I. I.; Briggs, D. P.; Valentine, J. Dielectric
44
45 Meta-Reflectarray for Broadband Linear Polarization Conversion and Optical Vortex
46
47 Generation. *Nano Lett.* **2014**, *14*, 1394-1399.
48
49
50
51
52
53
54
55
56
57
58
59
60

- 1
2
3
4 (29) Huang, L.; Chen, X.; Mühlenbernd, H.; Li, G.; Bai, B.; Tan, Q.; Jin, G.; Zentgraf, T.;
5
6 Zhang, S. Dispersionless Phase Discontinuities for Controlling Light Propagation. *Nano*
7
8 *Lett.* **2012**, *12*, 5750-5755.
9
- 10 (30) Lin, D.; Fan, P.; Hasman, E.; Brongersma, M. L. Dielectric Gradient Metasurface
11
12 Optical Elements. *Science* **2014**, *345*, 298-302.
13
- 14 (31) Liu, Z.; Li, Z.; Liu, Z.; Cheng, H.; Liu, W.; Tang, C.; Gu, C.; Li, J.; Chen, H. T.; Chen,
15
16 S.; Tian, J. Single-Layer Plasmonic Metasurface Half-Wave Plates with
17
18 Wavelength-Independent Polarization Conversion Angle. *ACS Photonics* **2017**, *4*,
19
20 2061-2069
21
22
23
24
- 25 (32) Zhao, Q.; Zhou, J.; Zhang, F.; Lippens, D. Mie Resonance-based Dielectric
26
27 Metamaterials. *Mater. Today* **2009**, *12*, 60-69.
28
29
- 30 (33) Jahani, S.; Jacob, Z. All-Dielectric Metamaterials. *Nat. Nanotechnol.* **2016**, *11*, 23-36.
31
32
- 33 (34) Gerchberg, R. W. A Practical Algorithm for the Determination of the Phase from Image
34
35 and Diffraction Plane Pictures. *Optik* **1972**, *35*, 237-246.
36
37
- 38 (35) Shimobaba, T.; Ito, T. Random Phase-Free Computer-Generated Hologram. *Opt.*
39
40 *Express* **2015**, *23*, 9549-9554.
41
- 42 (36) Dorsch, R. G.; Lohmann, A. W.; Sinzinger, S. Fresnel Ping-pong Algorithm for
43
44 Two-Plane Computer-Generated Hologram Display. *Appl. Optics* **1994**, *33*, 869-875.
45
46
- 47 (37) Liu, L.; Zhang, X.; Kenney, M.; Su, X.; Xu, N.; Ouyang, C.; Shi, Y.; Han, J.; Zhang, W.;
48
49 Zhang, S. Broadband Metasurfaces with Simultaneous Control of Phase and Amplitude.
50
51 *Adv. Mater.* **2014**, *26*, 5031-5036.
52
53
54
55
56
57
58
59
60

- 1
2
3
4 (38) Wang, Q.; Zhang, X.; Plum, E.; Xu, Q.; Xu, Y.; Zhang, H.; Liao, Y.; Gu, J.; Han, J.;
5
6 Zhang, W. Polarization and Frequency Multiplexed Terahertz Meta-Holography. *Adv.*
7
8 *Optical Mater.* **2017**, *5*, 1700277.
9
10
11
12
13
14
15
16
17
18
19
20
21
22
23
24
25
26
27
28
29
30
31
32
33
34
35
36
37
38
39
40
41
42
43
44
45
46
47
48
49
50
51
52
53
54
55
56
57
58
59
60

Figure Caption

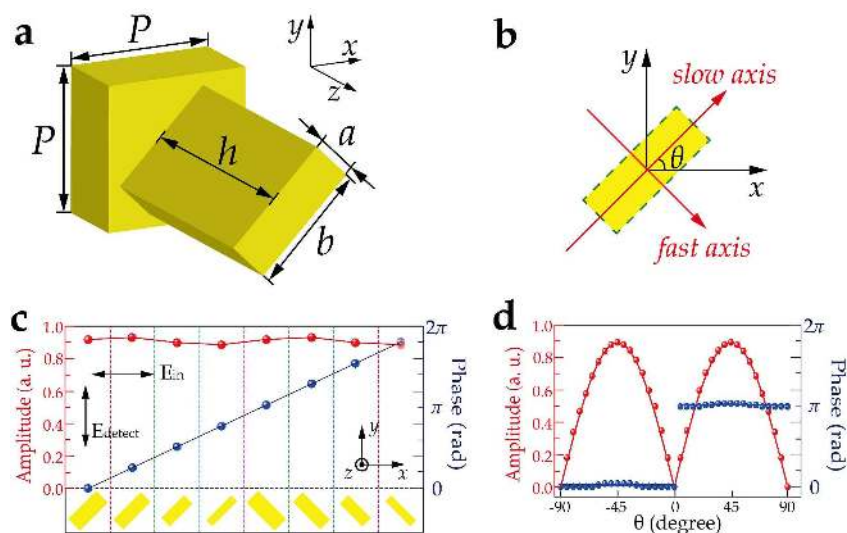


Figure 1. Illustration of the basic functional unit cells. (a) Schematic of a silicon pillar resonator patterned on a silicon substrate. a , b , and h represent the width, length, and thickness of the silicon pillar, respectively, and P represents the periodic size of the unit cell. (b) Schematic of the rotation of the silicon pillar. θ represents the orientation of the slow axis relative to the x -axis. (c) Numerically simulated transmission amplitude and phase shift of the y -polarized electric field component of the eight unit cells under 1.0 THz and an x -polarized normal incidence. (d) The same numerically simulated results as (c) for the first silicon pillar with $(a, b) = (48 \mu\text{m}, 115 \mu\text{m})$, as θ varies from -90° to 90° in a 5° interval. The amplitude shift follows a $|\sin(2\theta)|$ dependence (red solid line), while the phase shift remains constant except for a π jump at $\theta = 0^\circ$.

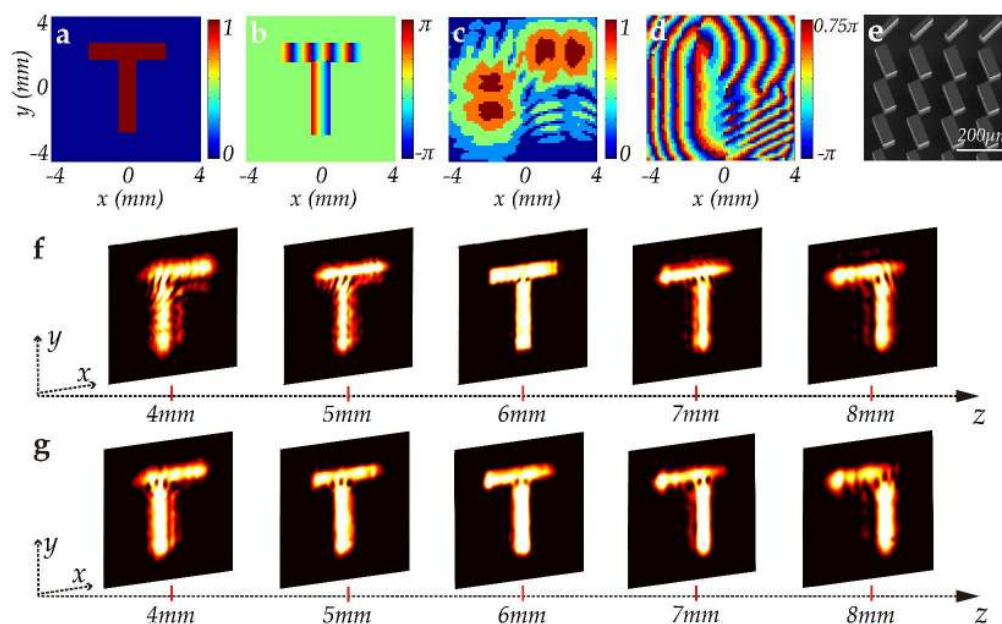


Figure 2. Illustration of the meta-hologram with controlled shifting along the z -axis. (a,b) The designed electric field amplitude and phase distributions of the virtual object at $z = 6$ mm, respectively. (c,d) The designed electric field amplitude and phase distributions of the meta-hologram, respectively, where five-level amplitude and eight-level phase modulation is adopted. (e) Scanning electron microscopy image of the dielectric meta-hologram with shifting manipulation (partial view). (f,g) Simulated and measured amplitude distributions of the y -polarized electric field component at 1.0 THz under an x -polarized normal incidence at different locations along the z -axis. All the observed regions are 8×8 mm².

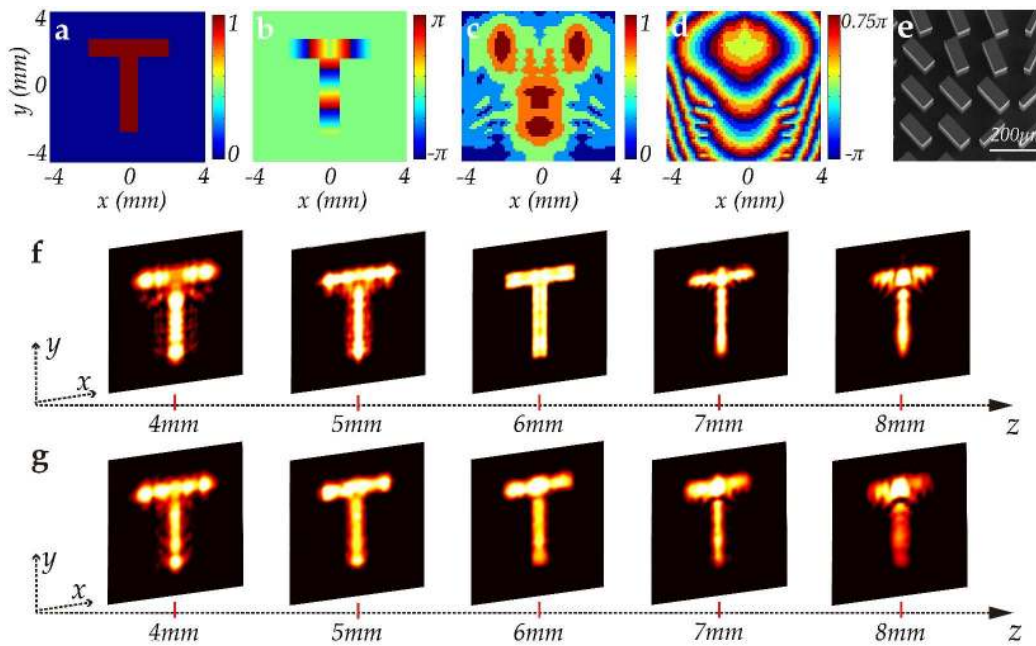


Figure 3. Illustration of the meta-hologram with controlled stretching along the z-axis.
(a-g) Similar results corresponding to Figure 2a-g, respectively.

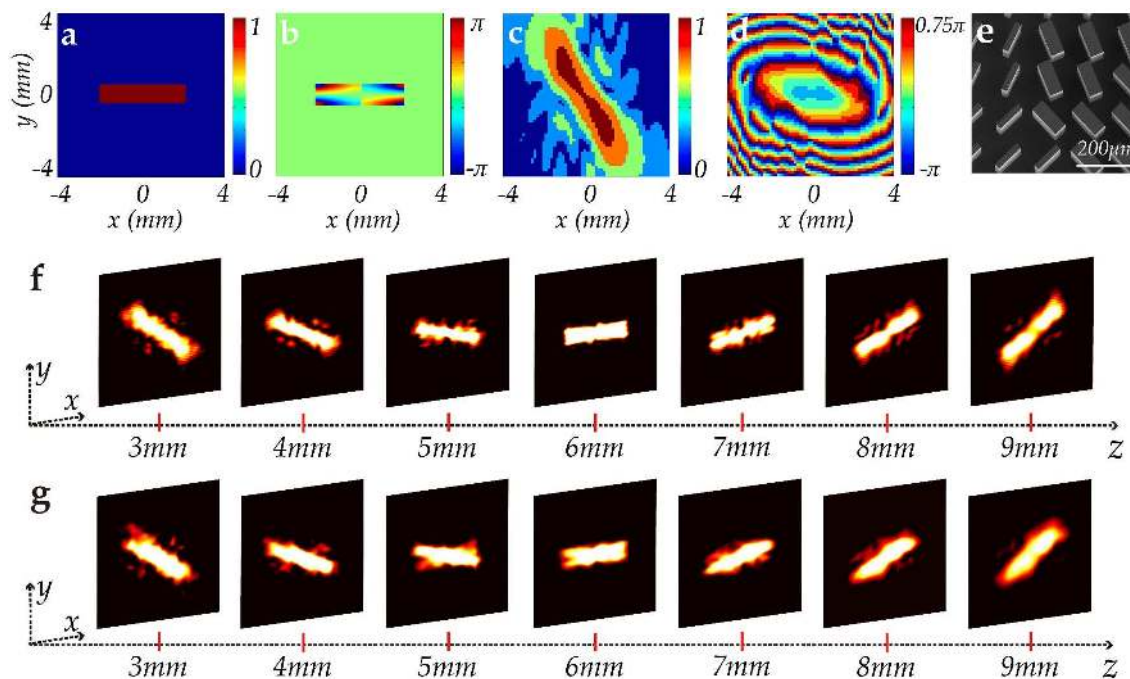


Figure 4. Illustration of the meta-hologram with controlled rotating along the z-axis.
(a-g) Similar results corresponding to Figure 2a-g, respectively.

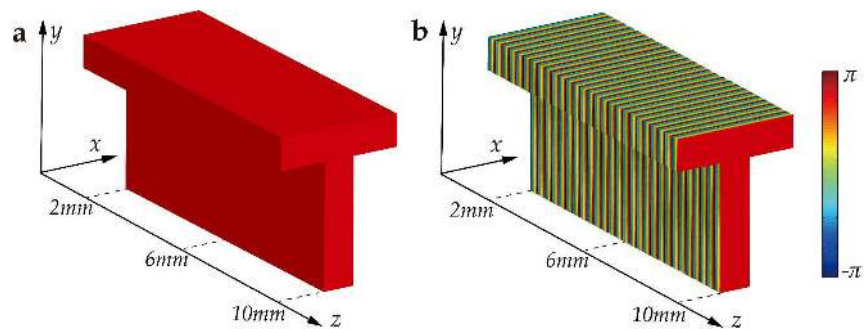


Figure 5. Illustration of the 3D designed meta-hologram. (a,b) The designed electric field amplitude and phase distributions of the 3D virtual object with z ranging from 2 to 10 mm. The sizes along the x and y directions are same as that in Figure 2a.

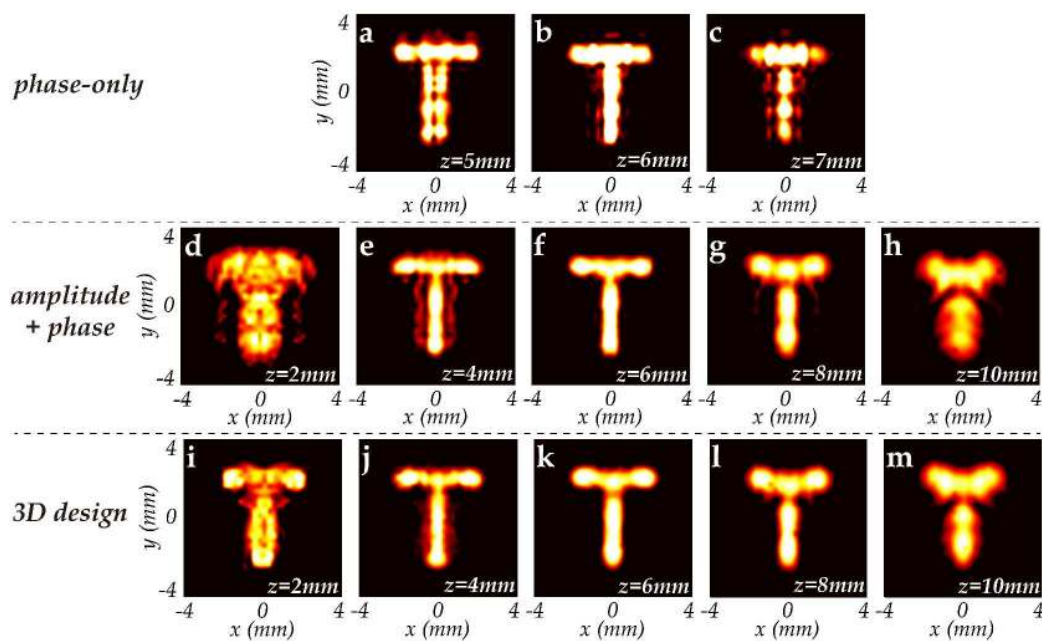


Figure 6. Experimental DOF characterization of the three meta-holograms. Measured electric field amplitude distribution at 1.0 THz at different locations along the z -axis, corresponding to (a-c) the phase-only meta-hologram, (d-h) the meta-hologram with simultaneous amplitude and phase control, and (i-m) the 3D designed meta-hologram with simultaneous amplitude and phase control. The location along the z -axis is shown at the bottom right corner of each figure.

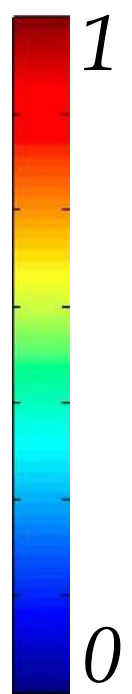
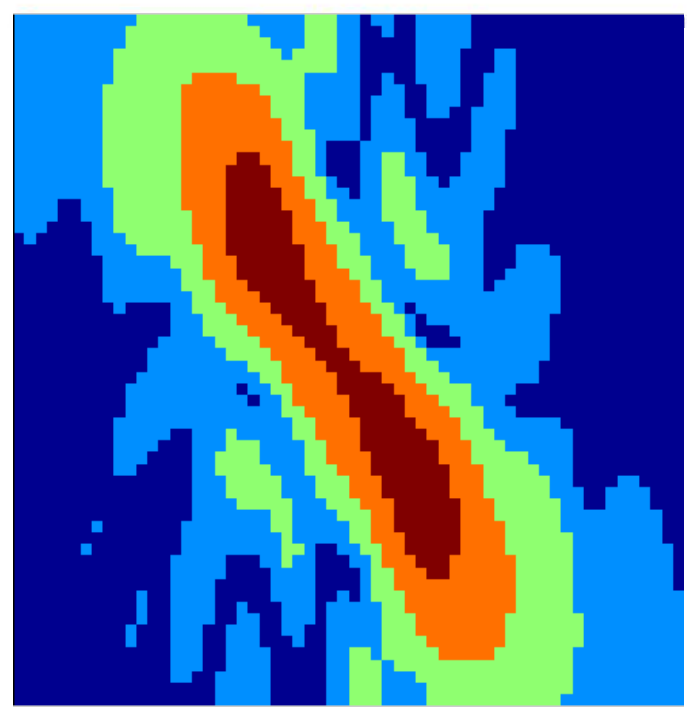
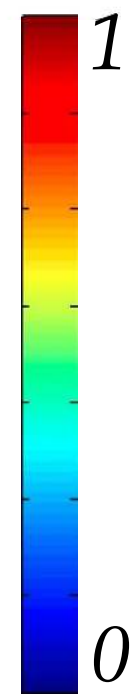
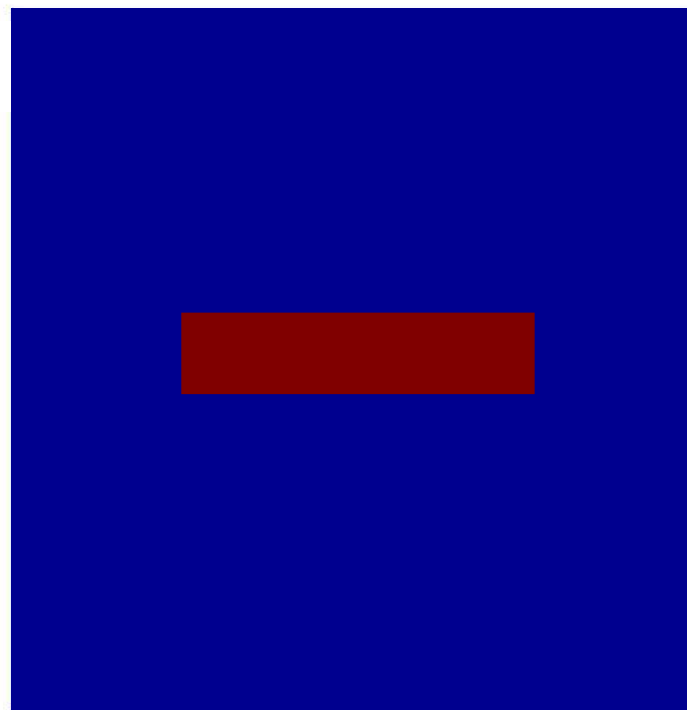
virtual object

meta-hologram

ACS Photonics

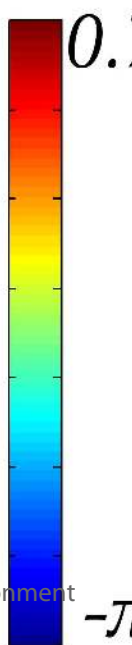
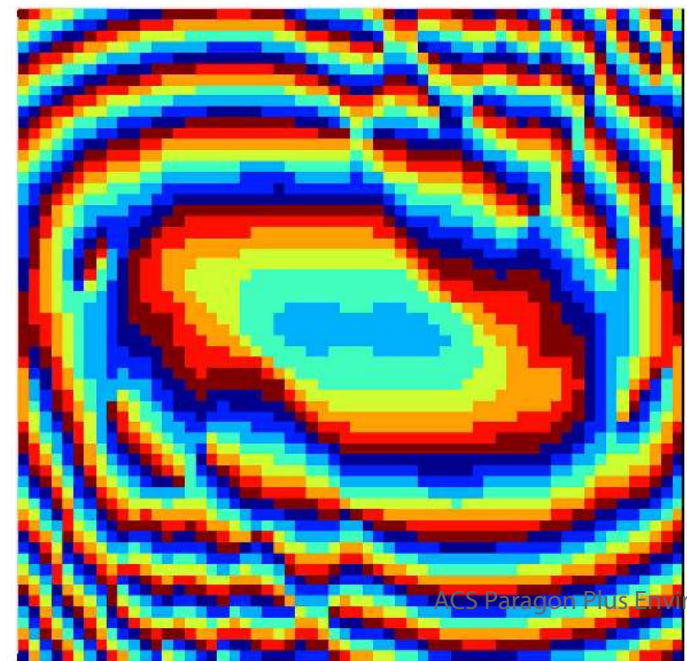
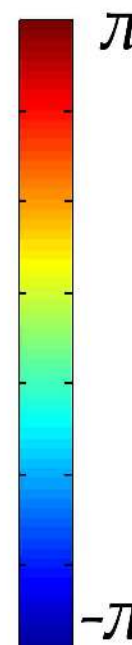
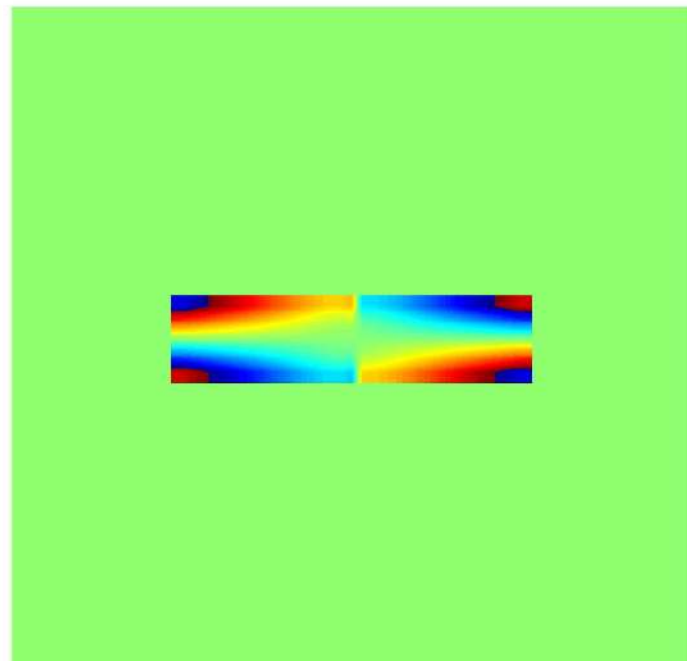
1
2
3
4
5
6
7
8
9
10
11
12
13
14
15
16
17
18
19
20
21
22
23
24

amplitude

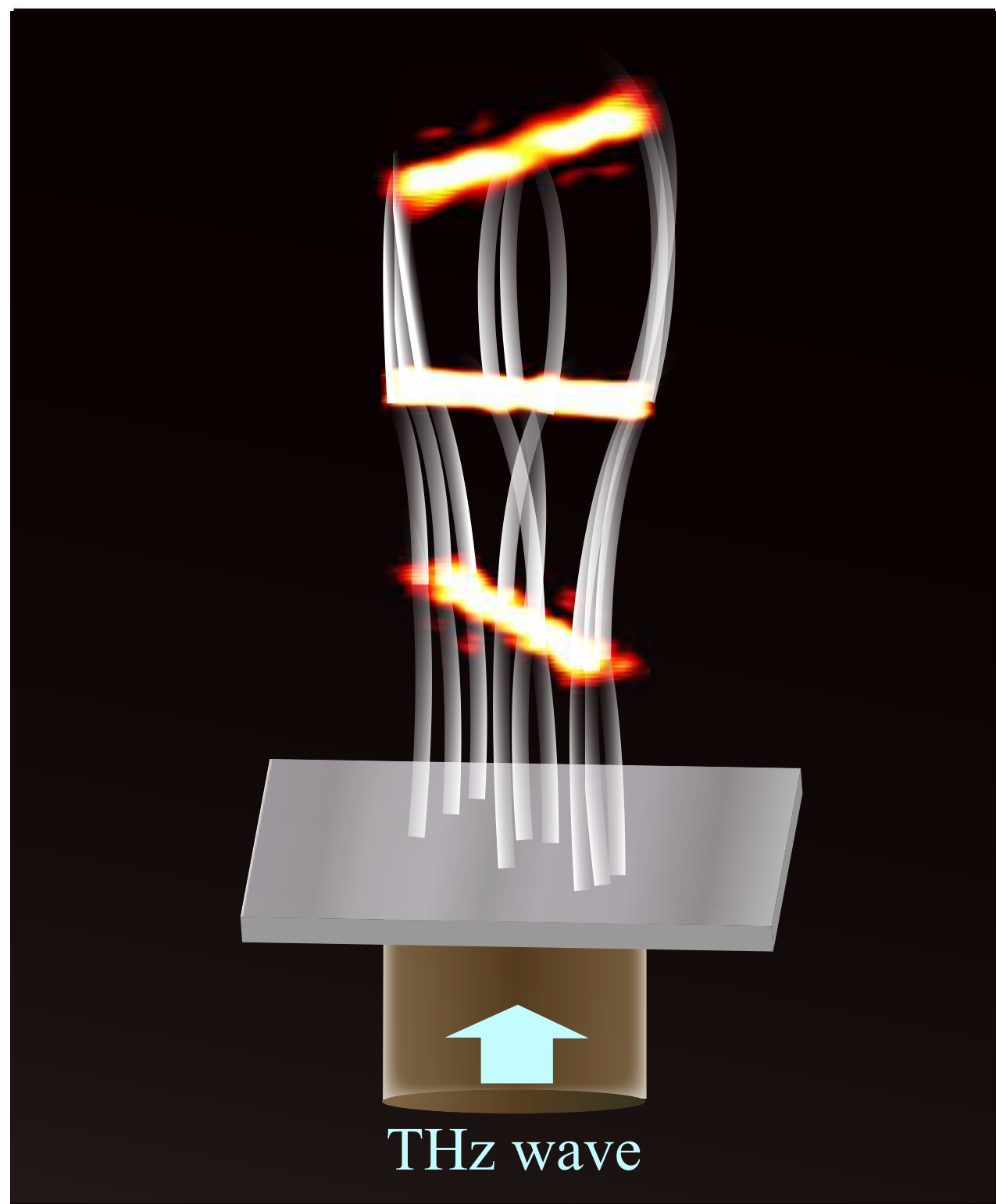


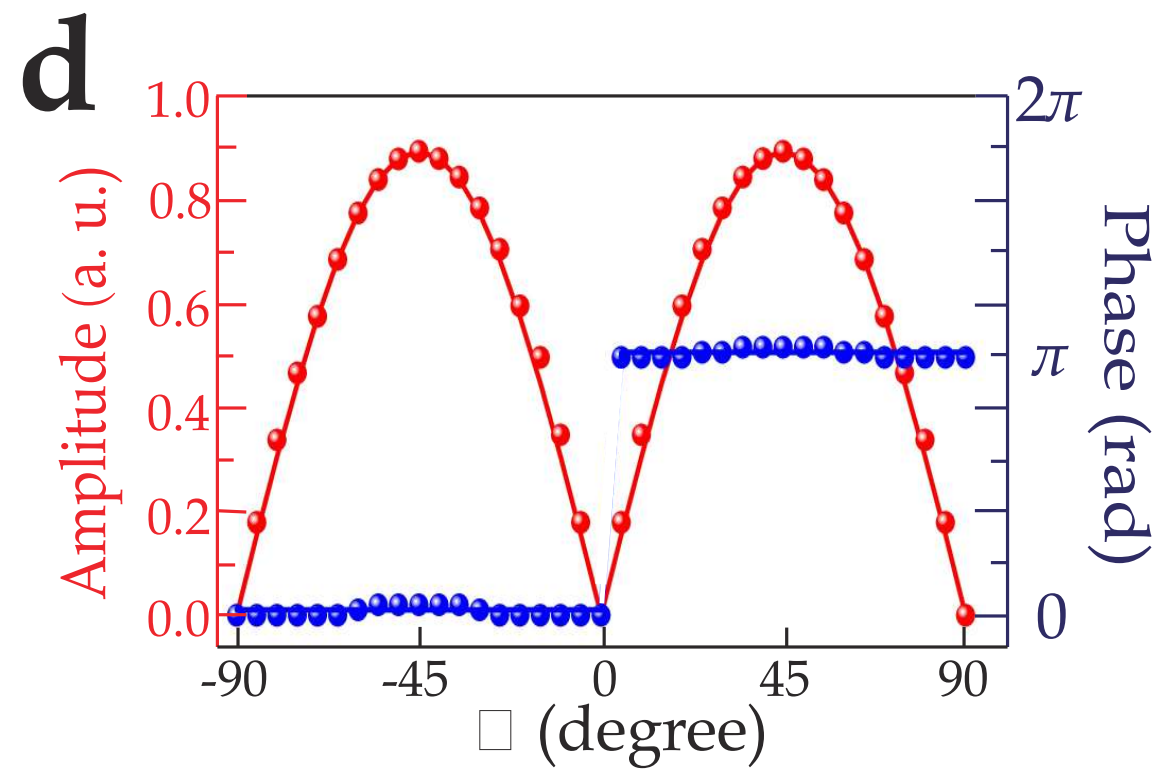
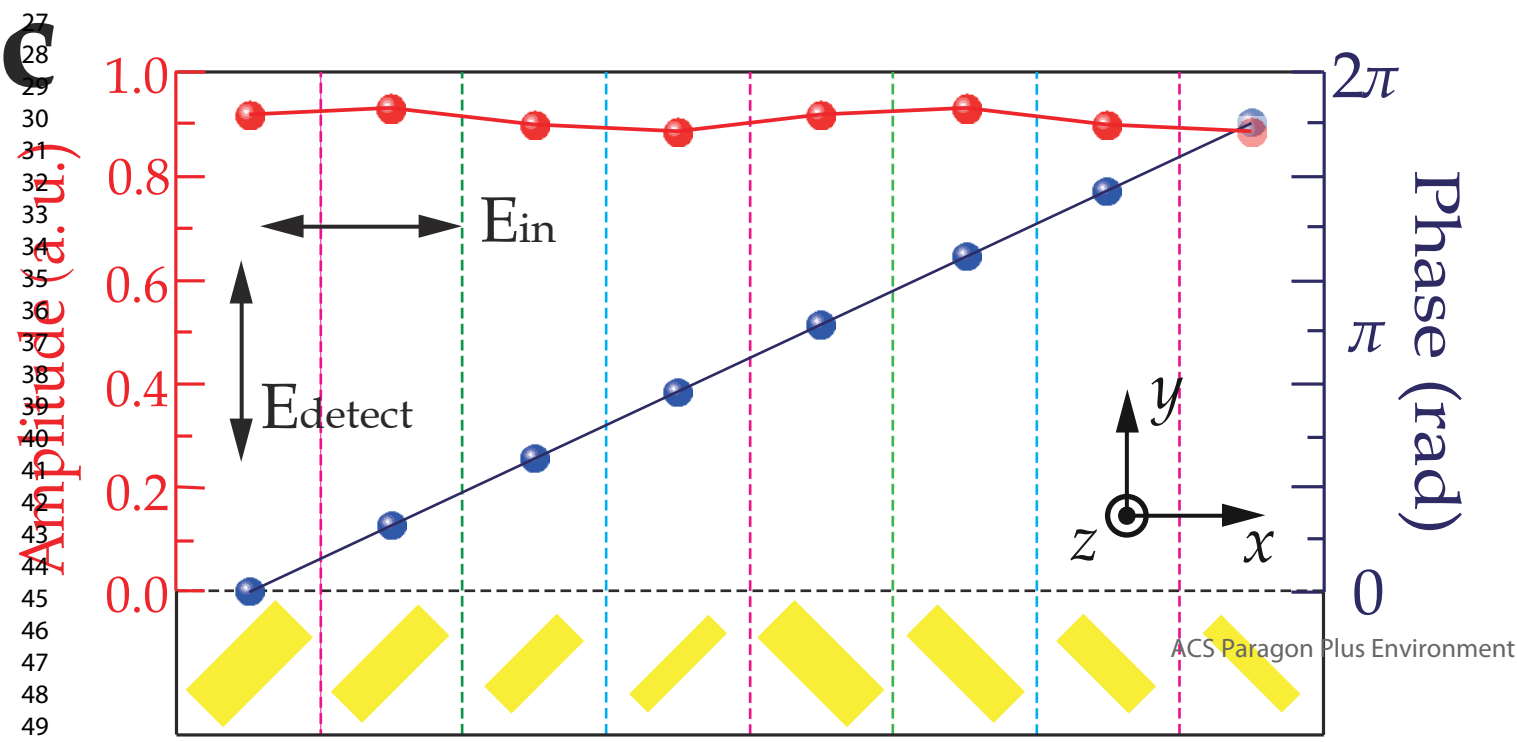
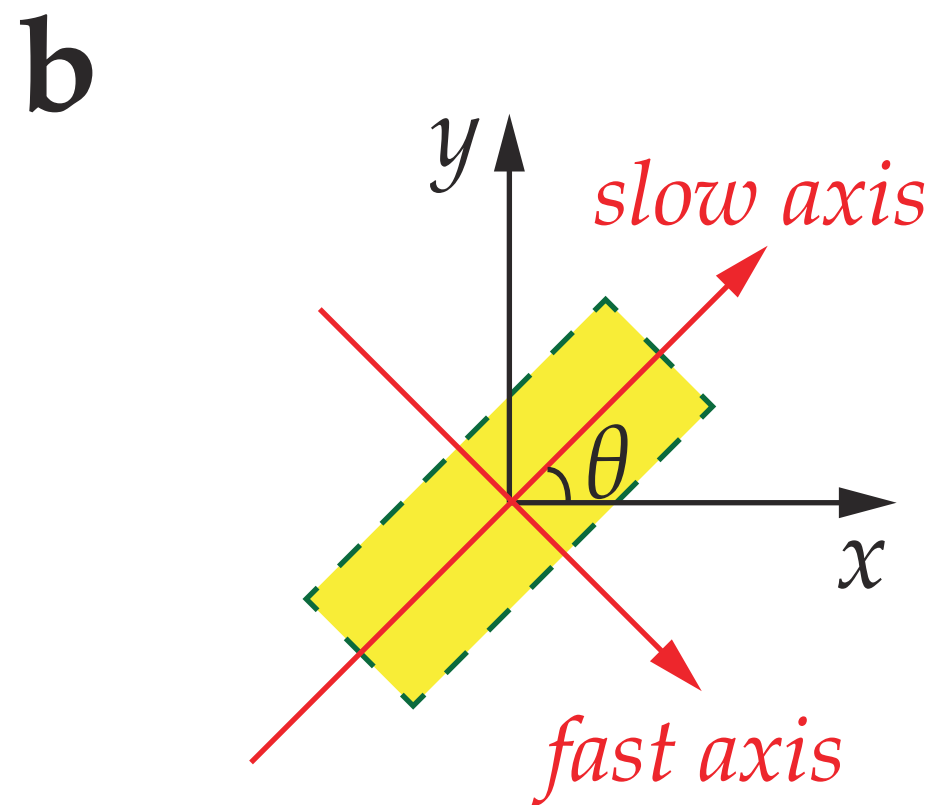
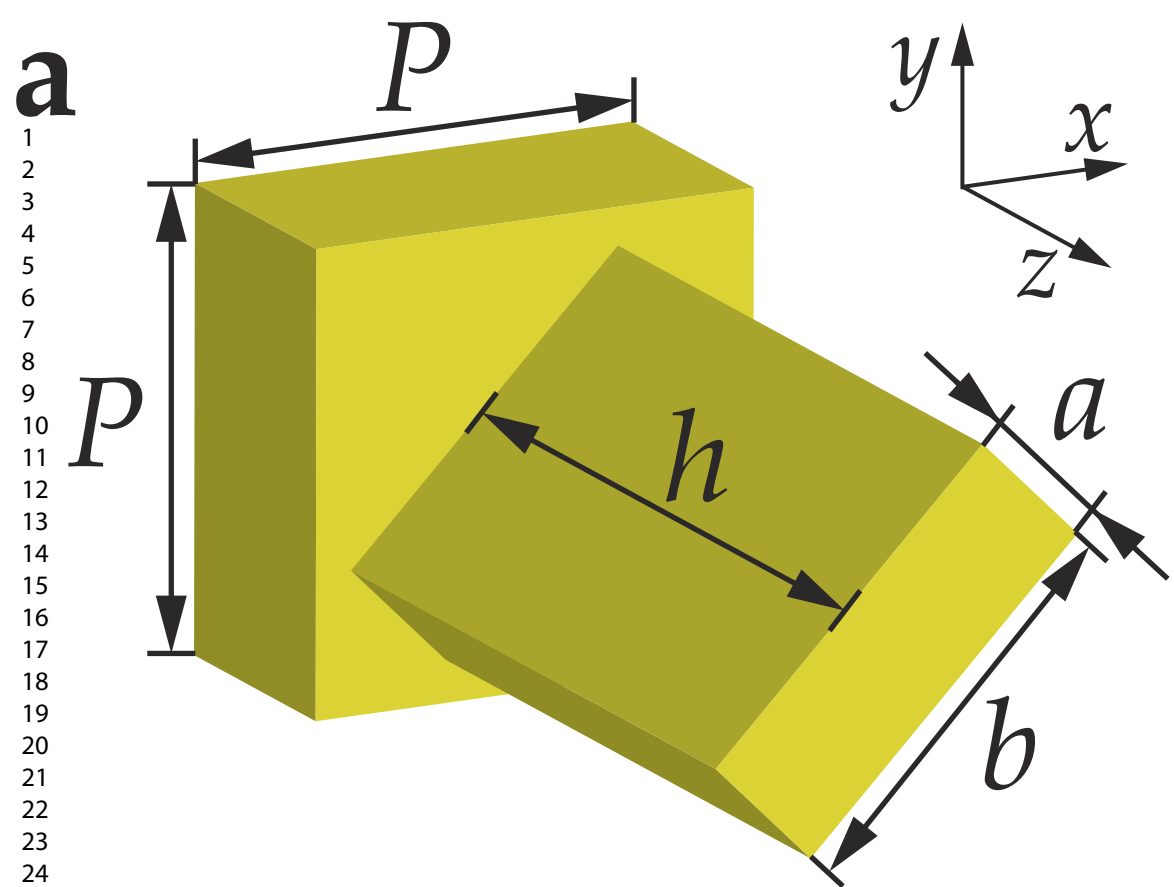
25
26
27
28
29
30
31
32
33
34
35
36
37
38
39
40
41
42
43
44
45
46
47

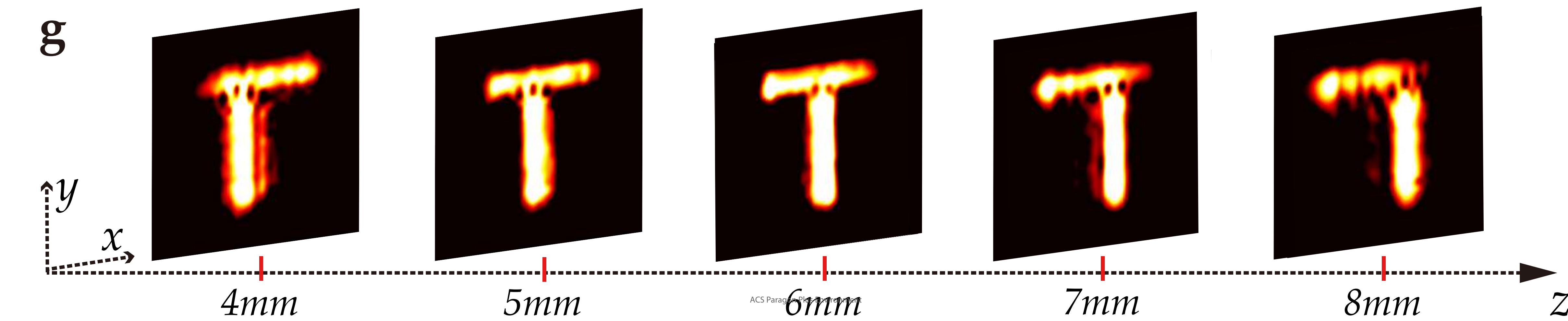
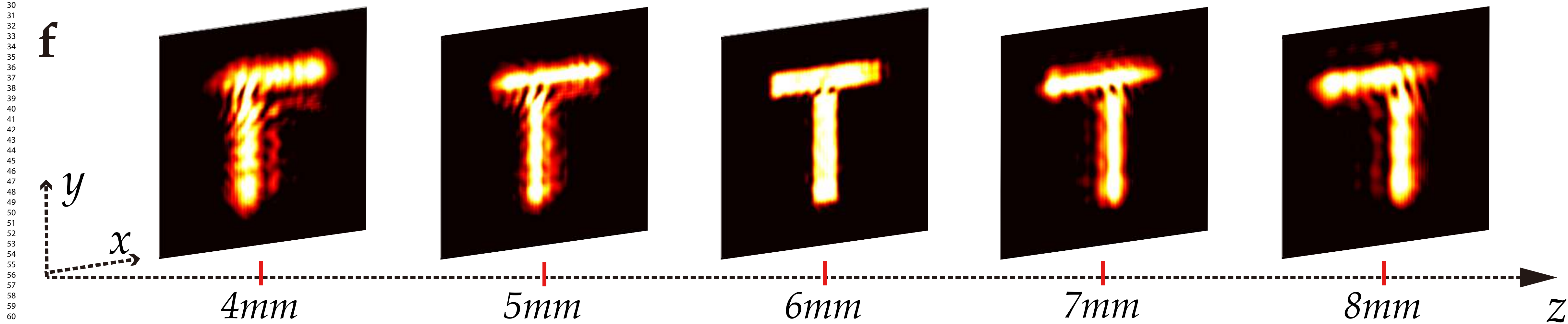
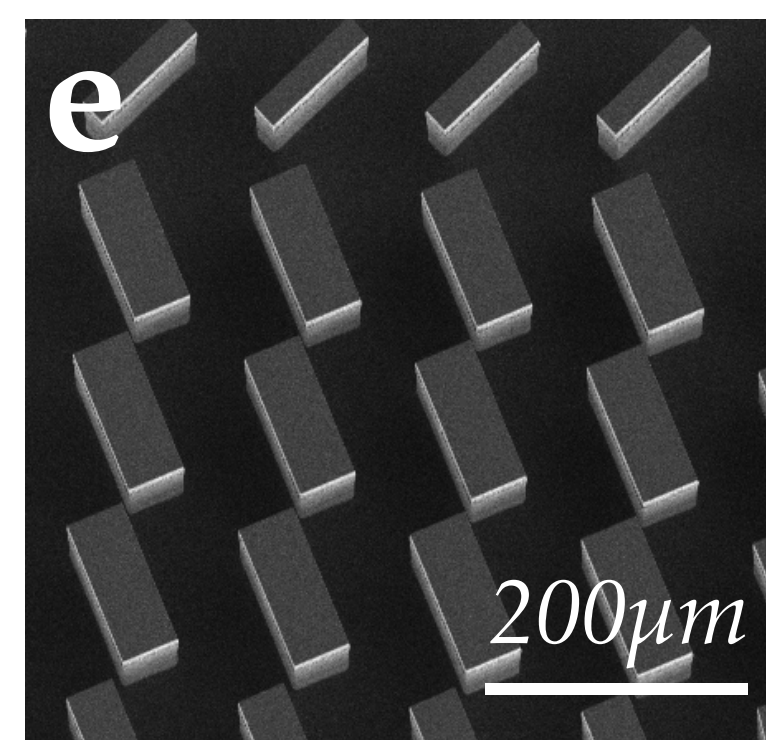
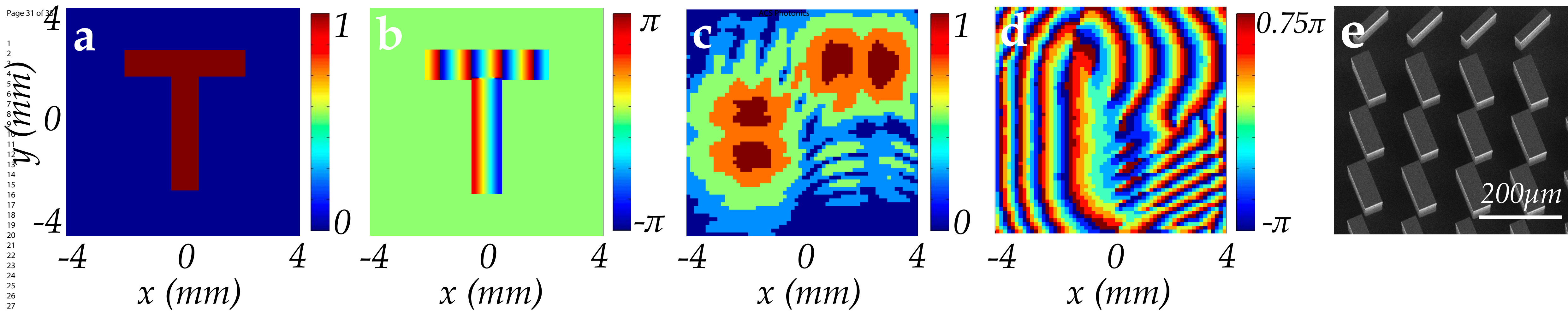
phase

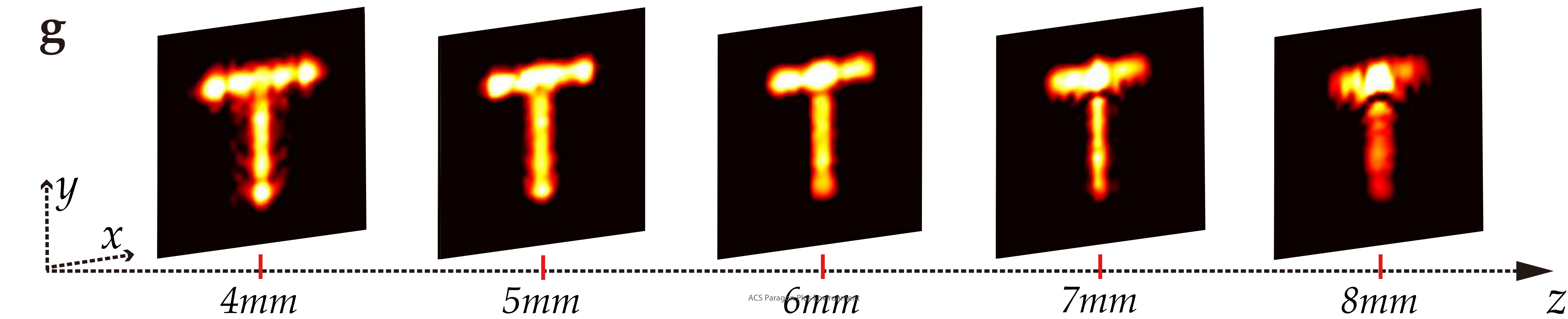
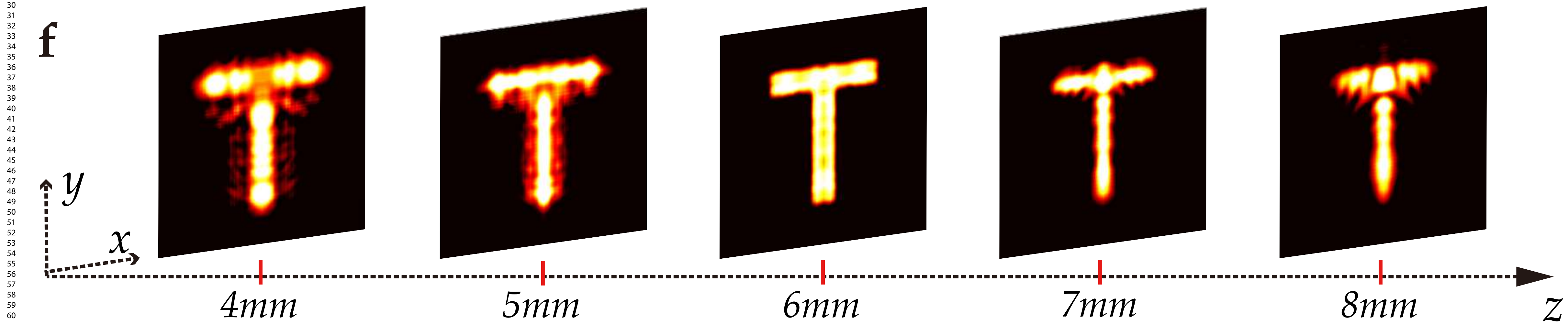
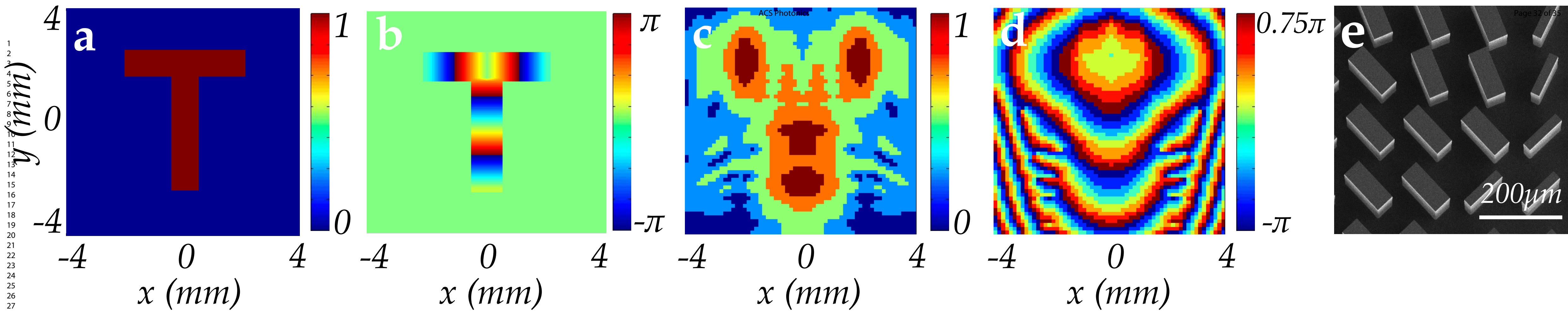


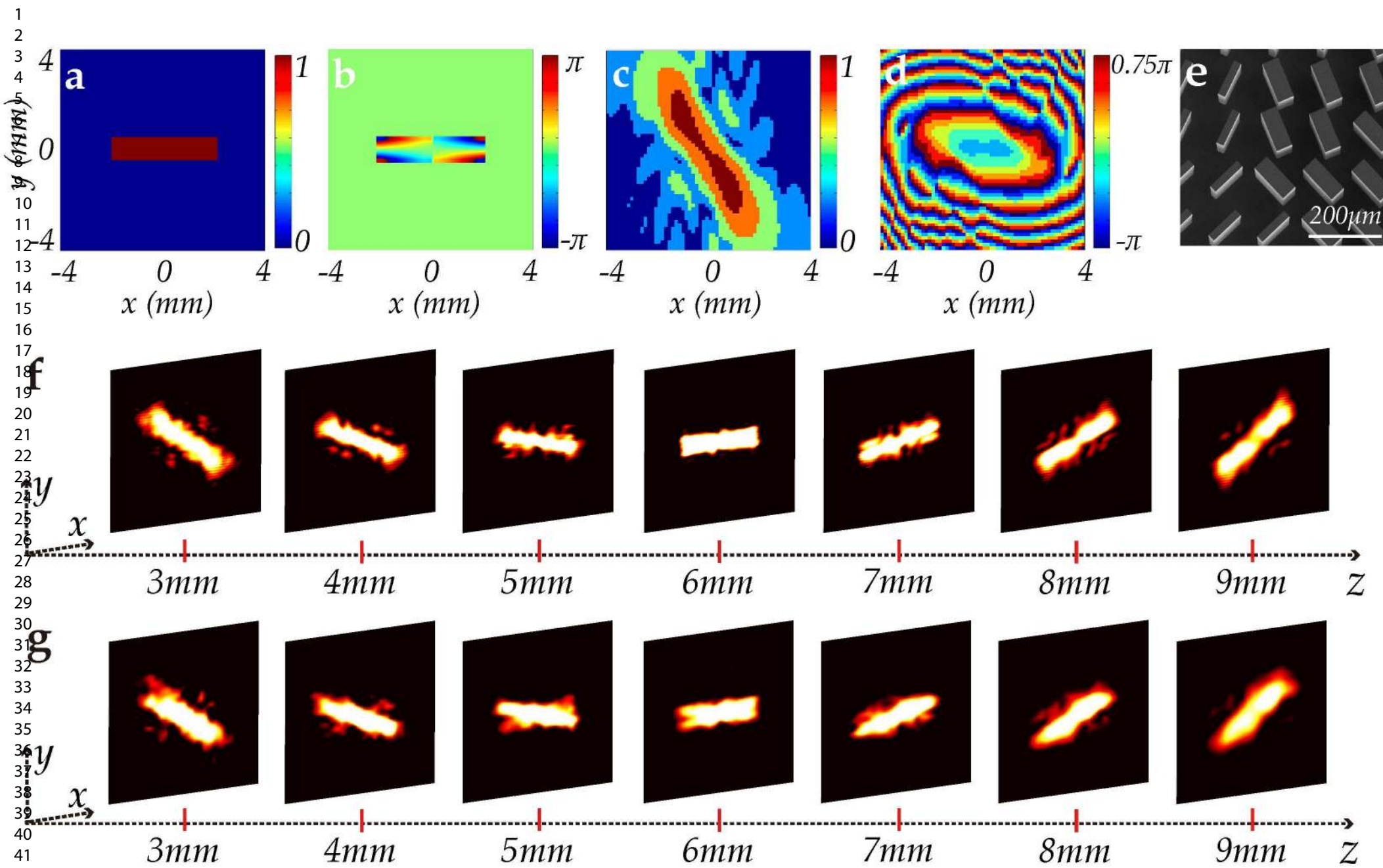
ACS Paragon Plus Environment

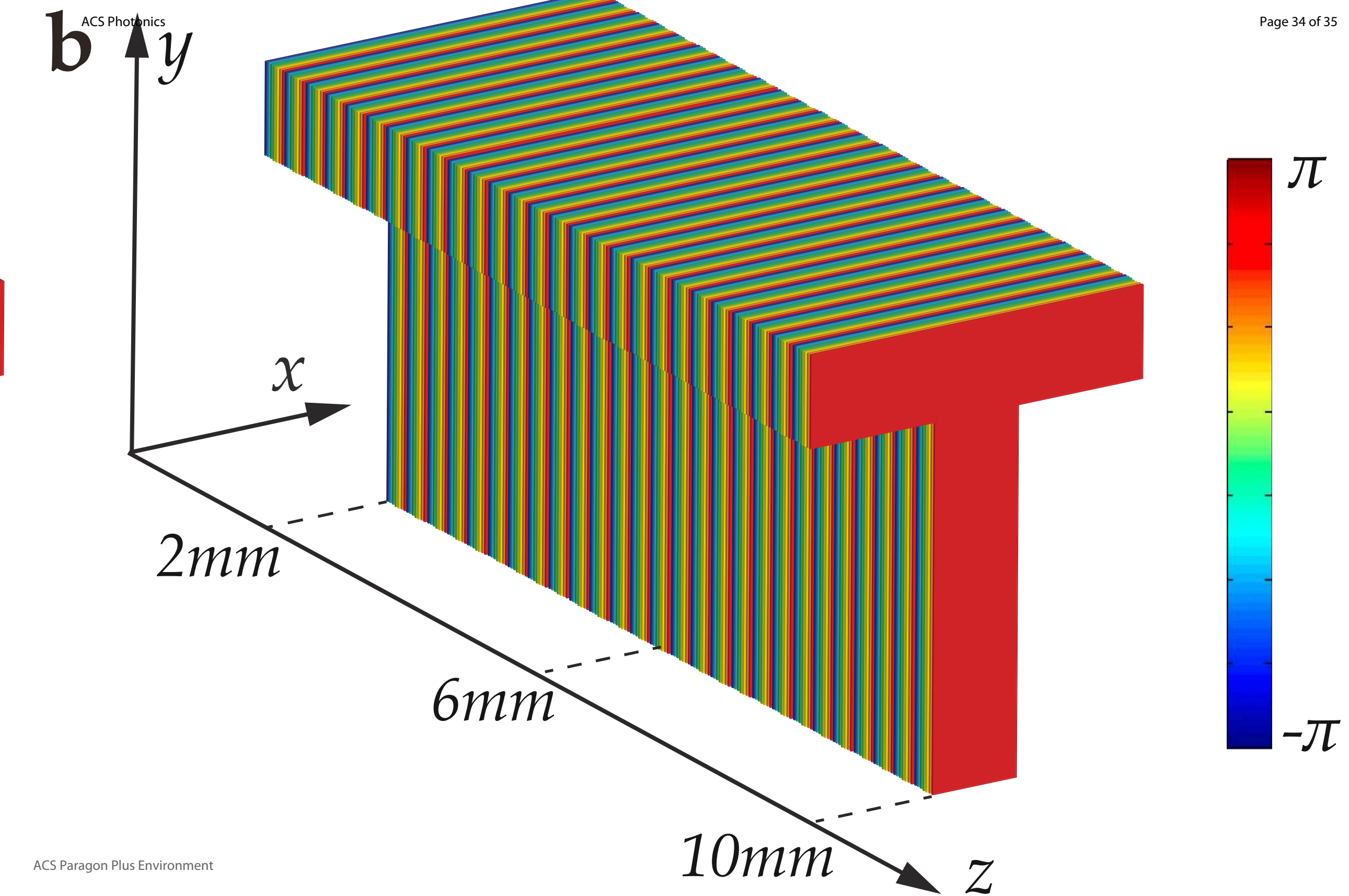
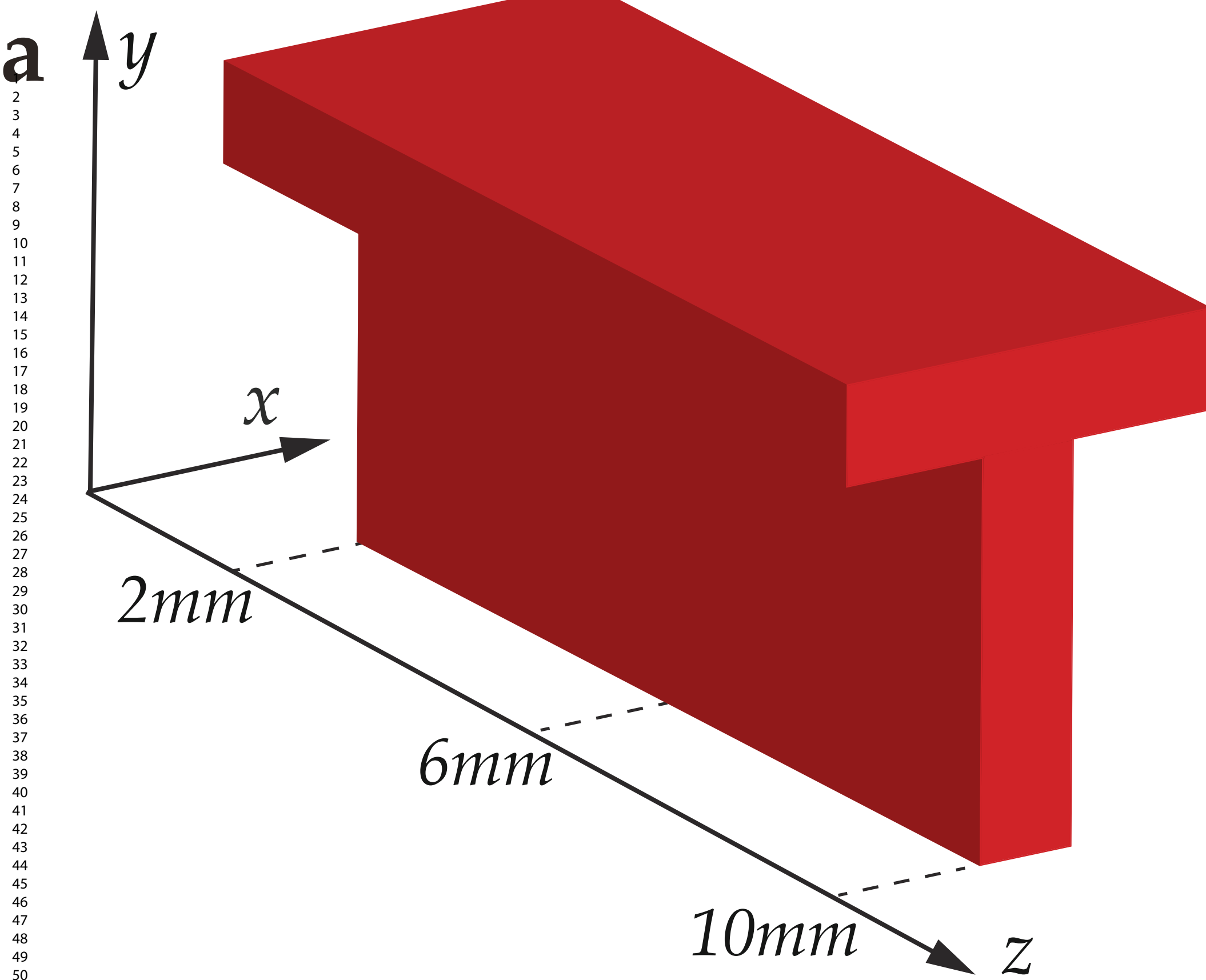






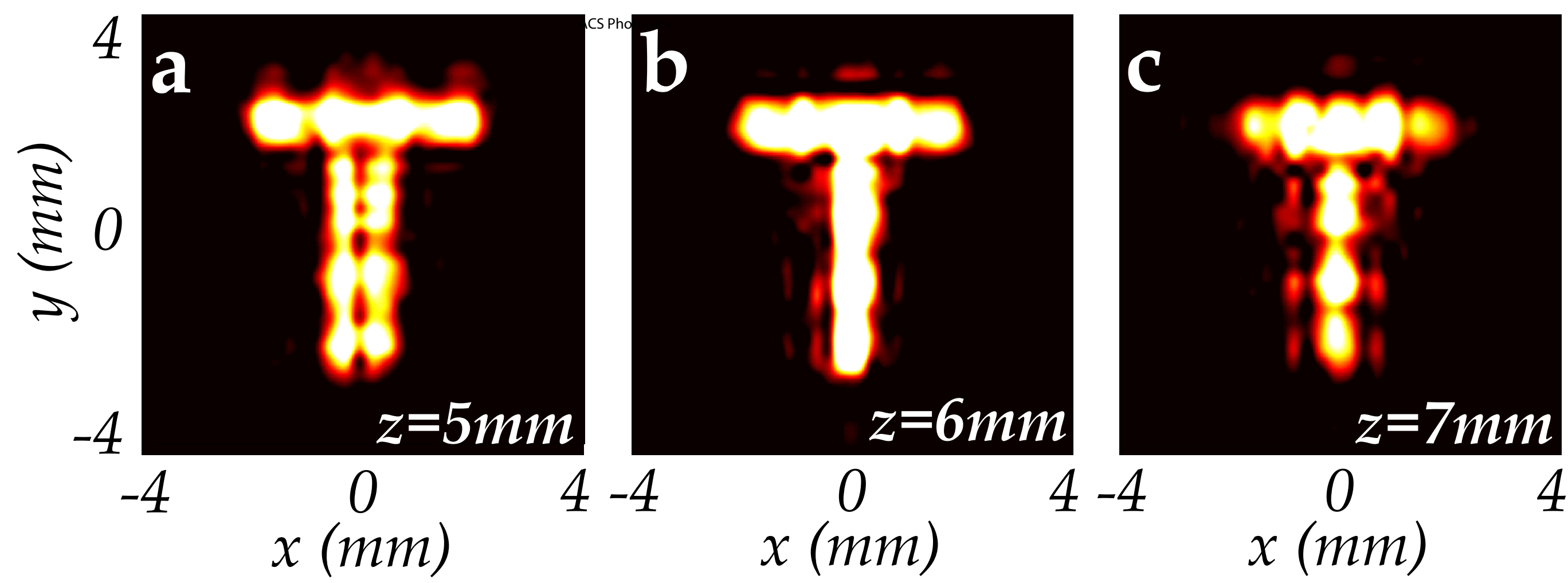




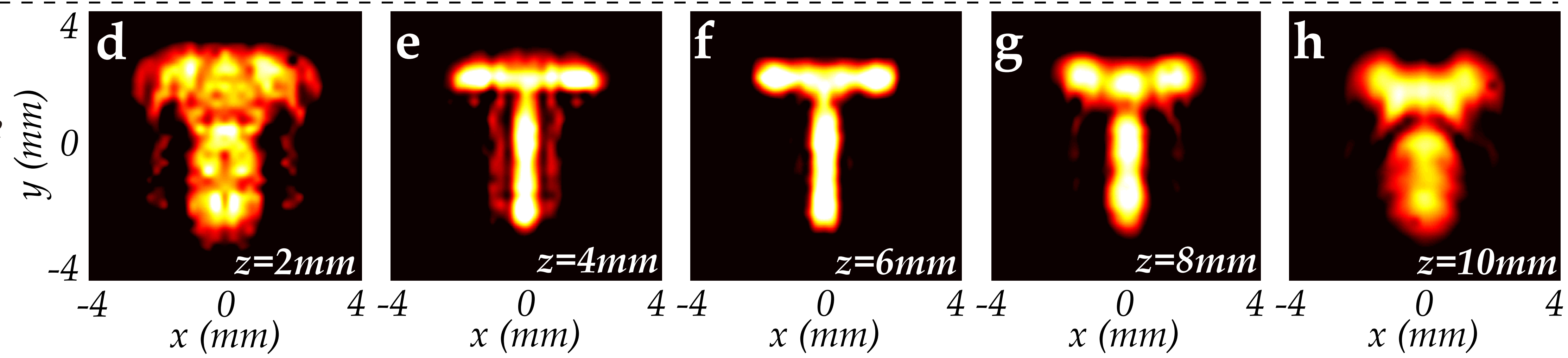


1
2
3
4
5
6
7
8
9
10
11
12
13
14
15
16
17
18
19
20
21
22
23
24
25
26
27
28
29
30
31
32
33
34
35
36
37
38
39
40
41
42
43
44
45
46
47
48
49
50
51
52
53
54
55
56
57
58
59
60

phase-only



amplitude + phase



3D design

